ELSEVIER

Computational Materials Science 28 (2003) 429–442

COMPUTATIONAL MATERIALS SCIENCE

www.elsevier.com/locate/commatsci

The effect of nanotube radius on the constitutive model for carbon nanotubes

H. Jiang [a], P. Zhang [b], B. Liu [a], Y. Huang [a,*], P.H. Geubelle [c], H. Gao [d], K.C. Hwang [e]

[a] *Department of Mechanical and Industrial Engineering, University of Illinois, 1206 W. Green Street, Urbana, IL 61801, USA*
[b] *Department of Mechanical Engineering, University of Connecticut, Storrs, CT 06269, USA*
[c] *Department of Aeronautical and Astronautical Engineering, University of Illinois, Urbana, IL 61801, USA*
[d] *Max Planck Institute for Metals Research, Heisenbergstrasse 3, D-70569 Stuttgart, Germany*
[e] *Department of Engineering Mechanics, Tsinghua University, Beijing 100084, China*

Abstract

We investigate the effect of nanotube radius on the constitutive model of single wall carbon nanotubes. We adopt a modified Cauchy–Born rule to incorporate the interatomic potential into the continuum analysis, and such an approach ensures the equilibrium of atoms. It is shown that the nanotube radius has little effect on the mechanical behavior of single wall carbon nanotubes subject to simple tension or pure torsion, while the nanotube orientation has somewhat larger influences.

Keywords: Nanotube radius; Carbon nanotube; Continuum; Constitutive model

1. Introduction

Interests in carbon nanotubes (CNTs) continue to grow since their first discovery [1]. CNTs possess many novel and unique properties—including structural perfection, low density, high stiffness and strength, and excellent electric properties and bio-compatibility. As a result, CNTs may have a wide range of technological applications such as nano-composites, nano-electro-mechanical systems (NEMS), nano-electronics, and drug delivery.

There has been extensive research on the mechanical properties of CNTs. Many experiments have been conducted to determine the elastic modulus of CNTs, using various methods involving transmission electron microscopy [2,3] atomic force microscopy [4–7], scanning electron microscopy [8], scanning force microscopy [9], micro Raman spectroscopy [10], or electric field-induced tension [11]. Though there are large scatterings in the reported elastic modulus of CNTs, they are all on the order of 1 tera-Pascal (TPa). Aside from experimental studies, atomistic simulation techniques have also been employed [12–27] to study the mechanical behavior of CNTs, and their findings

* Corresponding author. Tel.: +1-217-265-5072; fax: +1-217-244-6534.
E-mail address: huang9@uiuc.edu (Y. Huang).

0927-0256/$ - see front matter © 2003 Elsevier B.V. All rights reserved.
doi:10.1016/j.commatsci.2003.08.004

agree qualitatively with the experimental studies. However, applications of atomistic simulations are intrinsically limited by its time and length scales (on the orders of pico-second and nano-meter, respectively). In other words, it is practically unfeasible using atomistic simulations to study "large" systems which consist of thousands of CNTs (e.g., CNT-based electronics, CNT-reinforcing composites) or systems that have longer time spans. To overcome these limitations, it may be desirable to have a continuum theory linking atomic motion of CNTs with their macroscopic behavior.

There are some recent efforts to develop continuum theories directly from atomistic models for bulk materials [28–32], nanoscale thin films [33], and nanoscale membranes [34]. Zhang et al. [35–37] and Huang and Wang [38] have proposed a nanoscale continuum theory for CNTs incorporating the interatomic potential based on the modified Cauchy–Born rule [30,39–41]. The interactions between carbon atoms on a single wall CNT (one layer of carbon atoms) are described by Brenner's [42] interatomic potential for carbon. The continuum strain energy density is obtained by averaging the energy stored in atomic bonds over bond orientations. Utilizing the work-conjugate relation between the stress and strain, the stress and incremental modulus are derived from the strain energy density. It should be noted that no additional fitted parameter is involved in this approach (except for those introduced in Brenner's [42] interatomic potential), and the results based this nanoscale continuum theory agree very well with Yakobson et al.'s [43] and Cornwell and Wille's [16] molecular dynamic simulations of CNTs.

However, Zhang et al. [35,36,44] have not accounted for the effect of CNT radius on the constitutive model for CNTs. This is because the interaction between each atom and its nearest neighbors are evaluated within the tangential plane of the CNTs (similar to a graphene sheet) in Zhang et al.'s studies. This is a good approximation for CNTs with large radii, but may not hold for small CNTs that have few atoms in the circumferential direction. The purpose of the present study is to investigate the effect of CNT radius on the constitutive behavior of CNTs.

In Section 2, the modified Cauchy–Born rule is presented in order to establish the constitutive model for CNTs accounting for the effect of CNT radius. The equilibrium equation for a single wall CNT is obtained in Section 3 by integrating the standard cylindrical equilibrium equation over the vanishing CNT thickness. Sections 4 and 5 show the effect of CNT radius on a single wall CNT in simple tension and in pure torsion, respectively. It is shown that the CNT radius has little effect on the mechanical behavior of CNTs. Therefore, the simple constitutive model of [35,36], which neglects the effect of radius, can be used for CNTs.

2. A constitutive model for single wall carbon nanotubes accounting for the effect of nanotube radius

We first summarize Brenner's [42] interatomic potential for carbon, from which we establish the constitutive model for CNTs accounting for the effect of CNT radius.

2.1. The interatomic potential for carbon

Brenner [42] suggested that a multi-body interatomic potential for a carbon bond as

$$V(r_{ij}) = V_R(r_{ij}) - B_{ij}V_A(r_{ij}), \tag{1}$$

where i and j denote the two carbon atoms at the ends of the bond, r_{ij} is the bond length (i.e., the distance between i and j); V_R and V_A are the pair terms (i.e., depending only on the bond length r_{ij}) that represent the repulsive and attractive interactions of the carbon atoms, and are given by

$$V_R(r) = \frac{D^{(e)}}{S-1}\,\mathrm{e}^{-\sqrt{2S}\beta(r-R^{(e)})}f_c(r), \tag{2}$$

$$V_A(r) = \frac{D^{(e)}S}{S-1}\,\mathrm{e}^{-\sqrt{\frac{2}{S}}\beta(r-R^{(e)})}f_c(r). \tag{3}$$

The parameters $D^{(e)}$, S, β and $R^{(e)}$ are determined by fitting with known physical properties of various types of carbon. In particular, $R^{(e)}$ represents the equilibrium distance of two freestanding carbon atoms (i.e., no other atoms). The values of these parameters, as well as others introduced in

Brenner's [42] interatomic potential, are given at the end of this section. The function f_c is merely a smooth cut-off function to limit the range of interaction between carbon atoms, and it is given by

$$f_c(r) = \begin{cases} 1 & r < R^{(1)}, \\ \frac{1}{2}\left\{1 + \cos\left[\frac{\pi(r-R^{(1)})}{R^{(2)}-R^{(1)}}\right]\right\} & R^{(1)} < r < R^{(2)}, \\ 0 & r > R^{(2)}, \end{cases} \tag{4}$$

where the effective range of the cut-off function is defined by $R^{(1)}$ and $R^{(2)}$. Specifically, $R^{(1)}$ and $R^{(2)}$ are chosen so as to account for interactions among only the nearest-neighbor carbon atoms.

The term B_{ij} in (1) represents a multi-body coupling term, which results from the interaction between atoms i, j and their local environment, and is given by

$$B_{ij} = \left[1 + \sum_{k(\neq i,j)} G(\theta_{ijk}) f_c(r_{ik})\right]^{-\delta}, \tag{5}$$

where k denotes the carbon atoms other than i and j, r_{ik} is the distance between carbon atoms i and k, the parameter δ is given at the end of this section, f_c is the aforementioned cut-off function in (4), and θ_{ijk} defines the angle between carbon bonds $i-j$ and $i-k$, as shown in Fig. 1. The function G is given by

$$G(\theta) = a_0\left[1 + \frac{c_0^2}{d_0^2} - \frac{c_0^2}{d_0^2 + (1+\cos\theta)^2}\right], \tag{6}$$

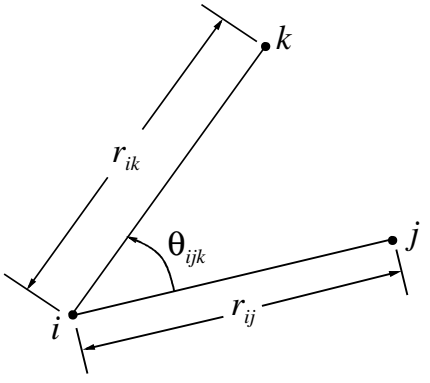

Fig. 1. Carbon atoms i, j, and k, the corresponding bonds $i-j$ and $i-k$, and bond angle θ_{ijk}.

where parameters a_0, c_0 and d_0 are also given at the end of this section.

Brenner [42] used the lattice constants and binding energies of graphite, diamond, simple cubic, and face-centered-cubic (fcc) carbon, as well as vacancy formation energies of graphite and diamond, to determine the parameters $D^{(e)}$, S, β, $R^{(e)}$, $R^{(1)}$, $R^{(2)}$, δ, a_0, c_0 and d_0 as

$$\begin{aligned} &D^{(e)} = 6.000 \text{ eV}, \quad S = 1.22, \quad \beta = 21 \text{ nm}^{-1}, \\ &R^{(e)} = 0.1390 \text{ nm}, \\ &R^{(1)} = 0.17 \text{ nm}, \quad R^{(2)} = 0.20 \text{ nm}, \\ &\delta = 0.50000, \\ &a_0 = 0.00020813, \quad c_0 = 330, \quad d_0 = 3.5. \end{aligned} \tag{7}$$

It is noted that the above interatomic potential is for pure carbon, though the Brenner potential [42] can also account for interaction with hydrogen atoms.

2.2. Single wall carbon nanotubes prior to deformation

Unlike a planar graphene sheet, a carbon atom and its three nearest-neighbor atoms on a CNT form a tetrahedron because of the curvature effect. Therefore, the carbon bonds on a CNT may have different lengths, depending on the bond orientation and the diameter of the CNT. Fig. 2a shows a cylindrical schematic diagram of a CNT with a diameter d_t prior to deformation. Since the CNT can be considered as a rolled graphene sheet, we map the CNT in Fig. 2a to the two-dimensional, planar sheet of carbon atoms in Fig. 2b. This mapping can be visualized by a cut of the CNT along its axial direction followed by the "unrolling" of the CNT to a plane without stretching. The distance between each pair of carbon atoms in the "unrolled" plane (Fig. 2b) is identical to the corresponding arc length on the CNT (Fig. 2a). However, we must point out that Fig. 2b is different from a graphene sheet since not only the bond lengths may not equal, but the bond angles may deviate from 120°. Fig. 2c shows a representative atom A in the "unrolled" plane along with its three nearest-neighbor atoms B, C, and D, which form a unit cell that can fill the entire plane

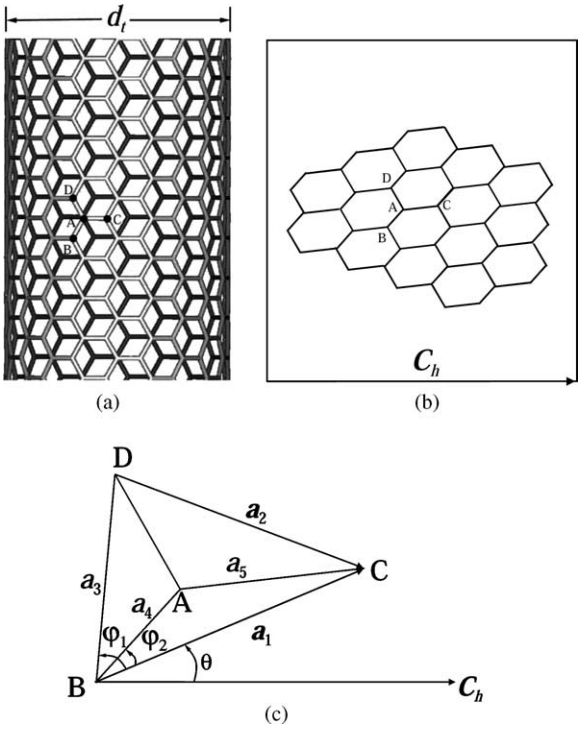

Fig. 2. A carbon nanotube (CNT) prior to deformation: (a) a CNT, (b) a planar, "unrolled" CNT, (c) a representative atom (A) and its three nearest-neighbor atoms (B, C, and D).

in Fig. 2b. Let $\boldsymbol{a}_1$ and $\boldsymbol{a}_2$ denote the vector $\overrightarrow{BC}$ and $\overrightarrow{DC}$ in Fig. 2c, respectively, and a_1 and a_2 be the corresponding lengths. The length of BD is denoted by a_3, and the lengths of AB and AC are denoted by a_4 and a_5, respectively (Fig. 2c). Other lengths and angles in the "unrolled" plane are completely determined by $a_1, a_2, \ldots, a_5$. For example, two angles $\varphi_1 = \angle CBD$ and $\varphi_2 = \angle CBA$ (Fig. 2c), which are used in the following to characterize the mapping between the CNT and the "unrolled" plane, are given in terms of the above lengths a_i $(i = 1, 2, \ldots, 5)$ by

$$\varphi_1 = \cos^{-1}\frac{a_1^2 + a_3^2 - a_2^2}{2a_1a_3}, \qquad \varphi_2 = \cos^{-1}\frac{a_1^2 + a_4^2 - a_5^2}{2a_1a_4}. \tag{8}$$

In order to characterize the cylindrical geometry of the CNT, it is necessary to prescribe the CNT diameter d_t and the angle θ between $\overrightarrow{BC}$ and the chiral vector $\boldsymbol{C}_h$, where $\boldsymbol{C}_h$ denotes the circumferential direction of the CNT (Fig. 2c). In the cylindrical coordinates (R, Θ, Z) of the CNT prior to deformation, the radial coordinates of all atoms are $R_A = R_B = R_C = R_D = d_t/2$. Without losing generality, we may take the polar angle and axial coordinate of atom B as zero, $\Theta_B = Z_B = 0$. The axial coordinates of atoms A, C, and D equal to the projections of vectors $\overrightarrow{BA}$, $\overrightarrow{BC}$, and $\overrightarrow{BD}$ normal to the $\boldsymbol{C}_h$ direction (Fig. 2c), i.e.,

$$Z_A = a_4\sin(\varphi_2 + \theta), \quad Z_C = a_1\sin\theta, \quad Z_D = a_3\sin(\varphi_1 + \theta). \tag{9}$$

Similarly, the polar angles of atoms A, C, and D are related to the projections along the $\boldsymbol{C}_h$ direction (Fig. 2c), and are given by

$$\Theta_A = \frac{2a_4\cos(\varphi_2 + \theta)}{d_t}, \quad \Theta_C = \frac{2a_1\cos\theta}{d_t}, \quad \Theta_D = \frac{2a_3\cos(\varphi_1 + \theta)}{d_t}. \tag{10}$$

The CNT diameter d_t and angle θ (Fig. 2) are, in fact, related to the chirality (n, m) of the CNT. Following the standard notation for CNTs (e.g., [45]), the chiral vector $\boldsymbol{C}_h$, whose length equals the circumference of the CNT, can always be expressed in terms of the base vectors $\boldsymbol{a}_1$ and $\boldsymbol{a}_2$ as (Fig. 2c)

$$\boldsymbol{C}_h = n\boldsymbol{a}_1 + m\boldsymbol{a}_2, \tag{11}$$

where n and m are integers, $n \geqslant |m| \geqslant 0$, and the pair (n, m) is called the chirality of the CNT; $(n, 0)$ and (n, n) are called zigzag and armchair CNTs, respectively, while the general case $n > |m| > 0$ is called a chiral CNT. Using the fact $\boldsymbol{a}_1 \cdot \boldsymbol{a}_1 = a_1^2$, $\boldsymbol{a}_2 \cdot \boldsymbol{a}_2 = a_2^2$, and $2\boldsymbol{a}_1 \cdot \boldsymbol{a}_2 = a_1^2 + a_2^2 - a_3^2$, we find the circumference of the CNT as

$$|\boldsymbol{C}_h| = \sqrt{\boldsymbol{C}_h \cdot \boldsymbol{C}_h} = \sqrt{n^2a_1^2 + m^2a_2^2 + nm(a_1^2 + a_2^2 - a_3^2)}, \tag{12}$$

and the CNT diameter

$$d_t = \frac{|\boldsymbol{C}_h|}{\pi}. \tag{13}$$

The angle θ is similarly obtained in terms of the chirality (n, m) as

$$\theta = \cos^{-1}\frac{\boldsymbol{C}_h \cdot \boldsymbol{a}_1}{|\boldsymbol{C}_h| a_1} = \cos^{-1}\frac{n a_1^2 + \frac{m}{2}(a_1^2 + a_2^2 - a_3^2)}{a_1 |\boldsymbol{C}_h|}. \quad (14)$$

It is important to point out that the bond length and angle used to calculate the energy stored in an atomic bond via (1) should be evaluated for the cylindrical configuration of the CNT (Fig. 2a). For example, the bond length between two atoms X and Y $(X, Y = A, B, C, D)$ with coordinates $(\frac{d_t}{2}, \Theta_X, Z_X)$ and $(\frac{d_t}{2}, \Theta_Y, Z_Y)$ prior to deformation is given by

$$r_{XY}^{(0)} = \sqrt{\frac{d_t^2}{2}[1 - \cos(\Theta_Y - \Theta_X)] + (Z_Y - Z_X)^2}. \quad (15)$$

For a given chirality (n, m) of the CNT, the bond length in (15) as well as the energy $V(r_{AX})$ stored in bond AX $(X = B, C, D)$ are functions of $a_1, a_2, \ldots, a_5$, where V is Brenner's [42] multi-body interatomic potential in (1). These lengths a_i $(i = 1, 2, \ldots, 5)$ differ from the lattice constants of graphite and can be determined by minimizing the average energy associated with each atom, i.e.,

$$\frac{\partial}{\partial a_i}[V(r_{AB}) + V(r_{AC}) + V(r_{AD})] = 0, \quad i = 1, 2, \ldots, 5. \quad (16)$$

Table 1 gives the numerical results of bond lengths, angles, CNT diameter, and orientation (angle θ) prior to deformation for several zigzag $[(n, 0)]$, armchair $[(n, n)]$, and chiral $[(n, m), n > |m| > 0]$ CNTs. The bond lengths and angles agree well with Sánchez-Portal et al.'s [46] *ab initio* atomistic studies for (4,4), (5,5), (6,6), (8,8) and (10,10) armchair CNTs based on the pseudopotential density functional theory. The results for a graphene sheet are also presented in Table 1 in order to show the effect of CNT radius. It is observed that, for CNT diameters above 0.8 nm, the bond lengths and angles are essentially the same as those of graphene (within 1% difference) such that the CNT radius has essentially no effect. However, for the smallest CNT diameter around 0.4 nm, the bond angle change is around 6%, such that the effect of CNT radius is significant.

If we take a graphene sheet as the ground (i.e., zero energy) state, the energy increase per atom in a CNT is given by $\frac{1}{2}[V(r_{AB}) + V(r_{AC}) + V(r_{AD})] - \frac{3}{2}V(r_{\text{graphene}})$, where V is Brenner's [42] interatomic potential in (1) and $r_{\text{graphene}} = 0.145$ nm is the lattice constant of graphene. This energy increase per atom is shown versus the CNT radius in Fig. 3, together with Robertson et al.'s molecular dynamics simulation results [12] based on Brenner's [42] interatomic potential. It is observed that the present analysis agrees very well with the atomistic studies, even for the smallest CNT radius 0.2 nm in Fig. 3, corresponding to only six atoms in the circumferential direction. The energy increase scales with $1/R^2$ in Fig. 3 because both stress and strain are proportional to the curvature $1/R$ at small deformation.

2.3. Continuum description of deformed single wall carbon nanotubes

The continuum deformation measures of deformed CNTs can be related to the motion of many atoms via the Cauchy–Born rule [39,40]. The Cauchy–Born rule equates the strain energy at the continuum level to the energy stored in atomic bond. It also states that the atoms subject to a homogeneous deformation move according to a single mapping from the undeformed to deformed configurations. From the continuum level, this mapping is taken to be the deformation gradient $\boldsymbol{F} = \partial \boldsymbol{x}/\partial \boldsymbol{X}$, where $\boldsymbol{X}$ and $\boldsymbol{x}$ denote the positions of a material point in the undeformed and deformed configurations, respectively. A bond between a pair of atoms i and j in the undeformed configuration is described by a vector $\boldsymbol{r}_{ij}^{(0)} = r_{ij}^{(0)} \boldsymbol{n}_{ij}^{(0)}$, where $r_{ij}^{(0)}$ is the bond length and $\boldsymbol{n}_{ij}^{(0)}$ is unit vector of the bond direction. Upon deformation, the bond is described by

$$\boldsymbol{r}_{ij} = \boldsymbol{F} \cdot \boldsymbol{r}_{ij}^{(0)}. \quad (17)$$

Its length becomes

$$r_{ij} = \sqrt{\boldsymbol{r}_{ij} \cdot \boldsymbol{r}_{ij}} = r_{ij}^{(0)} \sqrt{1 + 2\boldsymbol{n}_{ij}^{(0)} \cdot \boldsymbol{E} \cdot \boldsymbol{n}_{ij}^{(0)}}, \quad (18)$$

where

$$\boldsymbol{E} = \tfrac{1}{2}(\boldsymbol{F}^T \cdot \boldsymbol{F} - \boldsymbol{I}) \quad (19)$$

Table 1
Bond lengths and angles prior to deformation

	Chirality (n,m)	Diameter d_t (nm)	θ (degree)	Bond lengths (nm)			Bond angles (degree)		
				$r_{AB}^{(0)}$	$r_{AC}^{(0)}$	$r_{AD}^{(0)}$	$\angle BAC^{(0)}$	$\angle BAD^{(0)}$	$\angle CAD^{(0)}$
Graphene	$n+m\to\infty$	∞		0.14507	0.14507	0.14507	120	120	120
Zigzag nanotubes	(30,0)	2.4021	0	0.14511	0.14511	0.14508	119.80	119.96	119.96
	(20,0)	1.6036	0	0.14516	0.14516	0.14510	119.55	119.92	119.92
	(10,0)	0.80771	0	0.14544	0.14544	0.14518	118.20	119.69	119.69
	(7,0)	0.57104	0	0.14586	0.14586	0.14528	116.28	119.40	119.40
	(5,0)	0.41522	0	0.14669	0.14669	0.14542	112.59	118.99	118.99
Armchair nanotubes	(18,18)	2.4950	29.991	0.14509	0.14511	0.14509	119.87	120.02	119.87
	(12,12)	1.6646	29.979	0.14511	0.14517	0.14511	119.70	120.04	119.70
	(6,6)	0.83564	29.919	0.14525	0.14549	0.14525	118.80	120.17	118.80
	(5,5)	0.69797	29.887	0.14533	0.14568	0.14533	118.27	120.26	118.27
	(4,4)	0.56071	29.833	0.14548	0.14604	0.14548	117.31	120.45	117.31
Chiral nanotubes	(25,9)	2.4425	14.786	0.14510	0.14511	0.14508	119.82	120.00	119.91
	(16,6)	1.5786	15.262	0.14514	0.14518	0.14510	119.57	120.01	119.79
	(9,3)	0.87112	13.794	0.14532	0.14544	0.14518	118.56	120.02	119.36
	(6,2)	0.58567	13.673	0.14564	0.14592	0.14531	116.72	120.07	118.61
	(4,2)	0.43355	18.702	0.14603	0.14675	0.14555	114.19	120.59	116.92

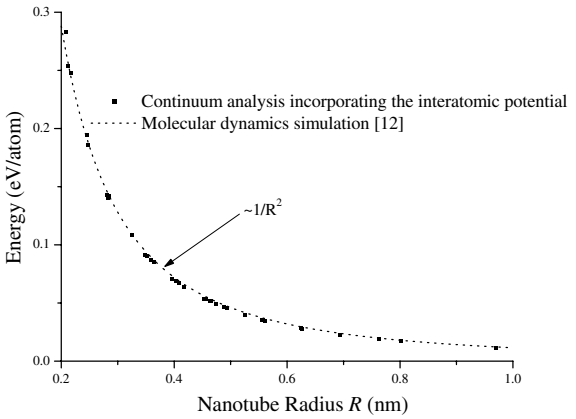

Fig. 3. The energy increase per atom in a carbon nanotube versus the nanotube radius R. A graphene sheet is taken as the ground state.

is the Lagrangian strain tensor and $\boldsymbol{I}$ is the second-order identity tensor. For a centrosymmetric lattice structure that has pair of bonds in the opposite directions ($\boldsymbol{r}$ and $-\boldsymbol{r}$) around each atom, the Cauchy–Born rule ensures the equilibrium of atoms because forces in the opposite, centrosymmetric bonds are always equal and opposite for arbitrarily imposed homogeneous deformation.

The deformation of a single wall CNT under simple tension and pure torsion is intrinsically two dimensional, represented by the Lagrangian strain components $E_{\Theta\Theta}$, E_{ZZ} and $E_{\Theta Z}$ $(= E_{Z\Theta})$ within the tangent plane of a CNT. For the deformed CNT whose cross-section remains circular as in simple tension or pure torsion, we may "unroll" the deformed CNT to a plane without stretching, similar to the mapping from Fig. 2a to b. It is shown in the Appendix that the sequence of first deforming the CNT and then mapping the deformed CNT to its "unrolled" plane is equivalent to mapping the undeformed CNT to its "unrolled" plane (as in Fig. 2a and b) followed by in-plane deformation according to $E_{11} = E_{\Theta\Theta}$, $E_{22} = E_{ZZ}$, and $E_{12} = E_{21} = E_{\Theta Z}$ $(= E_{Z\Theta})$, where the subscript "1" represents the circumferential direction $\boldsymbol{C}_h$ and "2" is normal to $\boldsymbol{C}_h$ in the plane. The deformed bond length of a CNT in a cylindrical configuration is then expressed in terms of the continuum deformation measures $E_{\Theta\Theta}$, E_{ZZ} and $E_{\Theta Z}$ $(= E_{Z\Theta})$.

The Cauchy–Born rule cannot be applied to CNTs because they do not have a centrosymmetric lattice structure, such that the Cauchy–Born rule cannot ensure the equilibrium of atoms anymore. Modifications of the Cauchy–Born rule for non-centrosymmetric lattice structures have been proposed [30,32,34–36,41]. Zhang et al. [35,36] applied the modified Cauchy–Born rule to CNTs, but did not account for the effect of CNT radius, which is studied in this paper.

Fig. 4 shows the plane "unrolled" from a deformed CNT. The hexagonal lattice can be decomposed into two triangular sub-lattices, marked by open circles and solid circles, respectively. The open-circle triangular sub-lattice, which consists of atoms B, C, D and the alike in Fig. 2c prior to deformation, possesses centrosymmetry such that the atoms in this sub-lattice follow the Cauchy–Born rule. The length between two atoms, such as B and C, on the "unrolled" plane for the deformed CNT is obtained from (18)

$$r_{BC}(\boldsymbol{E}) = \sqrt{\boldsymbol{r}_{BC}^{(0)} \cdot (\boldsymbol{I} + 2\boldsymbol{E}) \cdot \boldsymbol{r}_{BC}^{(0)}}, \tag{20}$$

where the dependence on the Lagrangian strain $\boldsymbol{E}$ is explicitly shown.

The solid-circle triangular sub-lattice in Fig. 4, which is composed of the atom A and the alike in

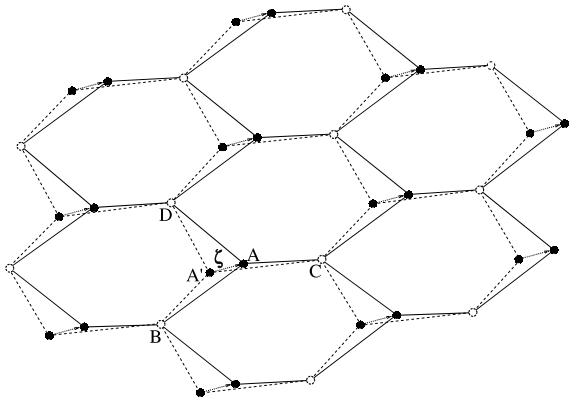

Fig. 4. The decomposition of a hexagonal lattice, "unrolled" from a deformed carbon nanotube, to two triangular sub-lattices. There is a shift vector $\boldsymbol{\zeta}$ between two sub-lattices to ensure the equilibrium of atoms. The solid and dashed lines denote the lattice structures with and without the shift vector $\boldsymbol{\zeta}$, respectively.

Fig. 2c prior to deformation, also possesses centrosymmetry. However, as shown in Fig. 4, the solid-circle sub-lattice may undergo a shift vector $\boldsymbol{\zeta}$ with respect to the open-circle sub-lattice in order to ensure the equilibrium of atoms. This shift vector $\boldsymbol{\zeta}$ affects the lengths between atoms from two sub-lattices. We may take the representative atom A and its three nearest-neighbor atoms B, C, and D to illustrate this. On top of the motion associated with the Cauchy–Born rule, the atom A is relaxed and moves additional $\boldsymbol{\zeta}$ relative to atoms B, C, and D such that the length AB, AC and AD are readjusted to ensure the equilibrium of atom A. The vector $\boldsymbol{r}_{AB}$ in Fig. 4 is the sum of $\boldsymbol{F}\cdot\boldsymbol{r}_{AB}^{(0)}$ (Cauchy–Born rule) and the shift vector $\boldsymbol{\zeta}$,

$$\boldsymbol{r}_{AB} = \boldsymbol{F}\cdot\boldsymbol{r}_{AB}^{(0)} + \boldsymbol{\zeta}. \tag{21}$$

Without losing generality, we may write $\boldsymbol{\zeta} = \boldsymbol{F}\cdot\boldsymbol{\xi}$, where $\boldsymbol{\xi} = \boldsymbol{F}^{-1}\cdot\boldsymbol{\zeta}$ is an internal degree of freedom to be determined by the equilibrium of atoms. The length r_{AB} is then given in terms of the Lagrangian strain $\boldsymbol{E}$ and the internal degree of freedom $\boldsymbol{\xi}$ by

$$\begin{aligned} r_{AB}(\boldsymbol{E},\boldsymbol{\xi}) &= \sqrt{\boldsymbol{r}_{AB}\cdot\boldsymbol{r}_{AB}} \\ &= \sqrt{(\boldsymbol{r}_{AB}^{(0)}+\boldsymbol{\xi})\cdot(\boldsymbol{I}+2\boldsymbol{E})\cdot(\boldsymbol{r}_{AB}^{(0)}+\boldsymbol{\xi})}, \end{aligned} \tag{22}$$

where the dependence on the Lagrangian strain $\boldsymbol{E}$ and the internal degree of freedom $\boldsymbol{\xi}$ is explicitly shown. Similar to (8)–(10) and (15), the bond lengths in the cylindrical configuration of a deformed CNT can be obtained in terms of $\boldsymbol{E}$ and $\boldsymbol{\xi}$ via the lengths in (20) and (22).

2.4. Linkage between the continuum strain energy density and the interatomic potential for single wall carbon nanotubes

The energy stored in an atomic bond AB, denoted by $V(r_{AB})$, is obtained from Brenner's [42] multibody interatomic potential in (1) once the bond lengths and angles are known for the cylindrical configuration of the deformed CNT. The energy for each representative atom A (Fig. 4) is given by $\frac{1}{2}[V(r_{AB})+V(r_{AC})+V(r_{AD})]$, where only the nearest-neighbor interactions between atoms are accounted for, and the factor $\frac{1}{2}$ results from the equal split of the energy between two atoms in the bond. The strain energy density W on the continuum level is the energy per unit area of the CNT surface, and is related to the interatomic potential by

$$W(\boldsymbol{E},\boldsymbol{\xi}) = \frac{V(r_{AB})+V(r_{AC})+V(r_{AD})}{2\Omega_{\varepsilon}}, \tag{23}$$

where the dependence on the Lagrangian strain $\boldsymbol{E}$ and the internal degree of freedom $\boldsymbol{\xi}$ is explicitly shown, Ω_{ε} is the undeformed CNT surface area per atom and is given by

$$\Omega_{\varepsilon} = \sqrt{s(s-a_1)(s-a_2)(s-a_3)}, \tag{24}$$

with $s=(a_1+a_2+a_3)/2$ (Fig. 2c). It can be shown that the strain energy density in (23) is independent of the choice of the representative atom (A).

The equilibrium of atoms is equivalent to the minimization of energy. The internal degree of freedom $\boldsymbol{\xi}$ is determined by minimizing the strain energy density $W(\boldsymbol{E},\boldsymbol{\xi})$ with respect to $\boldsymbol{\xi}$, i.e.,

$$\frac{\partial W}{\partial \boldsymbol{\xi}} = 0. \tag{25}$$

This gives an implicit equation to determine $\boldsymbol{\xi}$ in terms of the Lagrange strain $\boldsymbol{E}$, i.e., $\boldsymbol{\xi}=\boldsymbol{\xi}(\boldsymbol{E})$. The strain energy density is then written as

$$W = W[\boldsymbol{E},\boldsymbol{\xi}(\boldsymbol{E})]. \tag{26}$$

2.5. Stress and incremental modulus

The second Piola–Kirchhoff stress $\boldsymbol{T}$ is the work conjugate of the Lagrangian strain $\boldsymbol{E}$, and $\boldsymbol{T}$ is obtained from the total derivative of the strain energy density W with respect to $\boldsymbol{E}$,

$$\boldsymbol{T} = \frac{\mathrm{d}W}{\mathrm{d}\boldsymbol{E}} = \frac{\partial W}{\partial \boldsymbol{E}} + \frac{\partial W}{\partial \boldsymbol{\xi}}\cdot\frac{\partial \boldsymbol{\xi}}{\partial \boldsymbol{E}} = \frac{\partial W}{\partial \boldsymbol{E}}, \tag{27}$$

where (25) has been used. The incremental modulus tensor $\boldsymbol{C}$ is obtained by taking the total derivative of the second Piola–Kirchhoff stress $\boldsymbol{T}$ with respect to $\boldsymbol{E}$ as

$$\begin{aligned} \boldsymbol{C} &= \frac{\mathrm{d}\boldsymbol{T}}{\mathrm{d}\boldsymbol{E}} \\ &= \frac{\partial^2 W}{\partial \boldsymbol{E}\partial \boldsymbol{E}} - \frac{\partial^2 W}{\partial \boldsymbol{E}\partial \boldsymbol{\xi}}\cdot\left(\frac{\partial^2 W}{\partial \boldsymbol{\xi}\partial \boldsymbol{\xi}}\right)^{-1}\cdot\frac{\partial^2 W}{\partial \boldsymbol{\xi}\partial \boldsymbol{E}}. \end{aligned} \tag{28}$$

The linear elastic modulus of a single wall CNT along the axial direction Z can be obtained from the above incremental modulus tensor $\boldsymbol{C}$ for the infinitesimal deformation, i.e., $\boldsymbol{E} = 0$ and therefore $\boldsymbol{\xi} = 0$. Specifically, the "Young's modulus" along the axial direction of the CNT is $[C_{ZZZZ} - \frac{C_{ZZ\Theta\Theta}^2}{C_{\Theta\Theta\Theta\Theta}}]_{\boldsymbol{E}=0,\xi=0}$. However, it is important to point out that this "Young's modulus" is in fact the elastic modulus multiplied by the tube thickness since the energy density in (23) is the energy per unit surface area of the CNT. It is a common practice to assume the monoatomic layer thickness 0.335 nm of graphite as the CNT thickness though this estimate is more suitable for multi-wall CNTs than for single wall CNTs [47]. In order to avoid this choice of CNT thickness, we present the Young's modulus of CNT, normalized by that of graphene, versus the CNT diameter in Fig. 5a and b for zigzag and armchair CNTs, respectively. The tight-binding simulation results of [21] are also shown. It is observed that the present continuum analysis agrees well with the tight-binding simulations over a wide range of CNT diameter. The Young's modulus of zigzag CNTs decreases faster with the CNT diameter than armchair CNTs. As will be shown in Fig. 6 in the Section 4, zigzag CNTs in tension also display weaker material behavior than armchair CNTs.

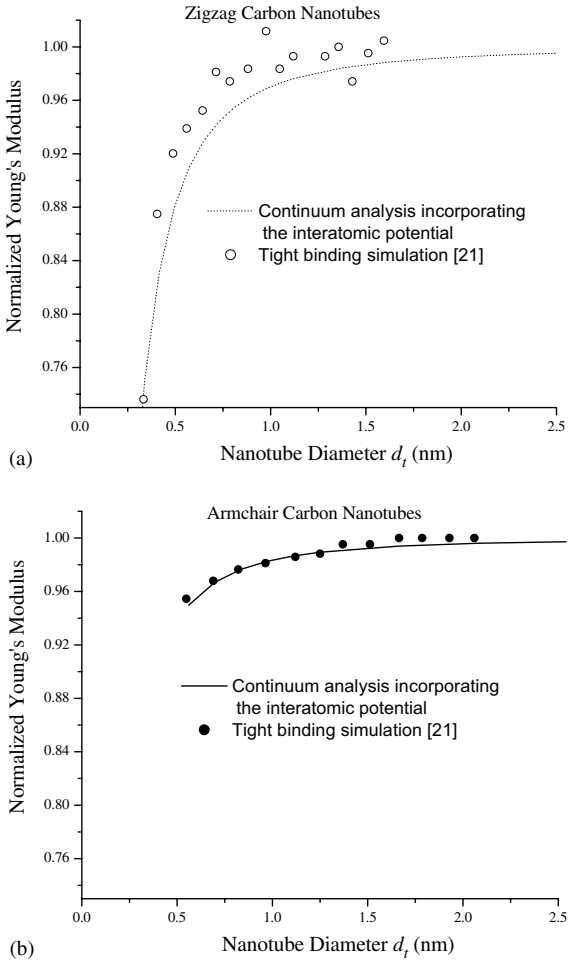

Fig. 5. The Young's modulus of carbon nanotubes (CNTs), normalized by that of the graphene, versus the nanotube diameter d_t for (a) zigzag CNTs, and (b) armchair CNTs.

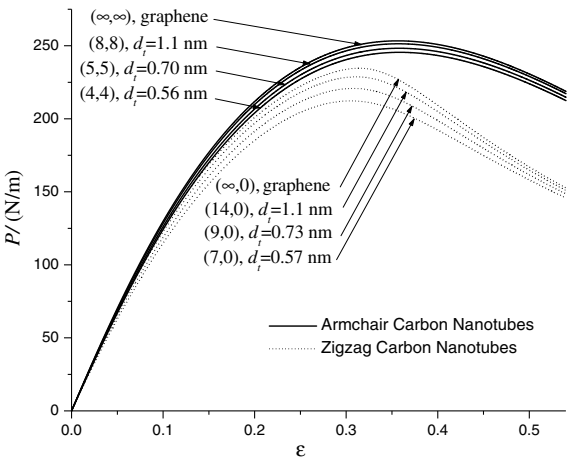

Fig. 6. The axial force P, normalized by the nanotube radius R prior to deformation, versus the engineering strain ε for several zigzag and armchair carbon nanotubes in simple tension. The diameter d_t of the carbon nanotube is given for each curve. The corresponding curves for graphene are also shown.

3. The equilibrium equation for single wall carbon nanotubes

The equilibrium equation for a single wall CNT is established in this section by integrating the standard cylindrical equilibrium equation over the vanishing thickness of the CNT. Let (R, Θ, Z) denote the cylindrical coordinates in the undeformed

configuration and $\boldsymbol{e}_R$, $\boldsymbol{e}_\Theta$, and $\boldsymbol{e}_Z$ the corresponding base vectors. The cylindrical equilibrium equation is

$$(\boldsymbol{F}\cdot\boldsymbol{T})\cdot\boldsymbol{\nabla}=0, \tag{29}$$

where $\boldsymbol{\nabla}=\boldsymbol{e}_R\frac{\partial}{\partial R}+\frac{\boldsymbol{e}_\Theta}{R}\frac{\partial}{\partial\Theta}+\boldsymbol{e}_Z\frac{\partial}{\partial Z}$ is the gradient operator. The traction-free boundary conditions on the inner and outer surfaces of the CNT are

$$\boldsymbol{F}\cdot\boldsymbol{T}\cdot\boldsymbol{e}_R=0. \tag{30}$$

The integration of (29) over the vanishing thickness of the CNT, in conjunction with the boundary condition (30), gives the following equilibrium equations for a single wall CNT

$$\frac{1}{R}\frac{\partial}{\partial\Theta}(\boldsymbol{F}\cdot\boldsymbol{T})_{R\Theta}-\frac{1}{R}(\boldsymbol{F}\cdot\boldsymbol{T})_{\Theta\Theta}+\frac{\partial}{\partial Z}(\boldsymbol{F}\cdot\boldsymbol{T})_{RZ}=0, \tag{31a}$$

$$\frac{1}{R}(\boldsymbol{F}\cdot\boldsymbol{T})_{R\Theta}+\frac{1}{R}\frac{\partial}{\partial\Theta}(\boldsymbol{F}\cdot\boldsymbol{T})_{\Theta\Theta}+\frac{\partial}{\partial Z}(\boldsymbol{F}\cdot\boldsymbol{T})_{\Theta Z}=0, \tag{31b}$$

$$\frac{1}{R}\frac{\partial}{\partial\Theta}(\boldsymbol{F}\cdot\boldsymbol{T})_{Z\Theta}+\frac{\partial}{\partial Z}(\boldsymbol{F}\cdot\boldsymbol{T})_{ZZ}=0, \tag{31c}$$

where R is the CNT radius in the undeformed configuration, $\boldsymbol{T}$ is the second Piola–Kirchhoff stress averaged over the CNT thickness and its non-vanishing components are $T_{\Theta\Theta}$, T_{ZZ}, and $T_{\Theta Z}$ $(=T_{Z\Theta})$.

4. A single wall carbon nanotube in simple tension

The shear stress vanishes in a single wall CNT subject to simple tension along its axial (Z) direction,

$$T_{\Theta Z}=T_{Z\Theta}=0. \tag{32}$$

Both the deformation gradient $\boldsymbol{F}$ and second Piola–Kirchhoff stress $\boldsymbol{T}$ are independent of Θ and Z such that the equilibrium equation (31a) gives

$$T_{\Theta\Theta}=0, \tag{33}$$

while (31b) and (31c) are satisfied automatically. Eqs. (32) and (33) can be written in terms of the strain energy density $W=W[\boldsymbol{E},\boldsymbol{\xi}(\boldsymbol{E})]=W(E_{\Theta\Theta},E_{ZZ},E_{\Theta Z}=E_{Z\Theta})$ as

$$\frac{\partial W}{\partial E_{\Theta Z}}=\frac{\partial W}{\partial E_{Z\Theta}}=0,\quad \frac{\partial W}{\partial E_{\Theta\Theta}}=0, \tag{34}$$

which gives two implicit equations to determine $E_{\Theta\Theta}$ and $E_{\Theta Z}$ $(=E_{Z\Theta})$ in terms of the axial strain E_{ZZ}. The shear strain $E_{\Theta Z}$ $(=E_{Z\Theta})$ always vanishes in zigzag $[(n,0)]$ and armchair $[(n,n)]$ CNTs in simple tension due to the symmetry of loading axis with respect to the lattice structure. It is noted that the two-step process of solving the shift vector $\boldsymbol{\xi}$ in terms of $\boldsymbol{E}$ from (25) and solving $E_{\Theta\Theta}$ and $E_{\Theta Z}$ $(=E_{Z\Theta})$ in terms of E_{ZZ} from (34) can be combined together by minimizing the strain energy density W simultaneously with respect to $\boldsymbol{\xi}$, $E_{\Theta\Theta}$ and $E_{\Theta Z}$ $(=E_{Z\Theta})$ via the standard minimization method.

The widely used engineering strain ε in simple tension (percentage of elongation) is related to the axial component of the Lagrangian strain E_{ZZ} by

$$E_{ZZ}=\tfrac{1}{2}(F_{ZZ}^2-1)=\tfrac{1}{2}[(1+\varepsilon)^2-1]=\varepsilon+\tfrac{1}{2}\varepsilon^2, \tag{35}$$

or equivalently,

$$\varepsilon=\sqrt{1+2E_{ZZ}}-1. \tag{36}$$

The axial force P on the CNT can be obtained by integrating the normal stress traction $\boldsymbol{e}_z\cdot(\boldsymbol{F}\cdot\boldsymbol{T}\cdot\boldsymbol{e}_Z)$ in the cross-section, which gives

$$P=2\pi RF_{ZZ}T_{ZZ}=2\pi R\sqrt{1+2E_{ZZ}}T_{ZZ}, \tag{37}$$

where T_{ZZ} is obtained from (27). Fig. 6 shows the axial force P, normalized by the CNT radius R prior to deformation, versus the engineering strain ε for four zigzag CNTs [(7,0), (9,0), (14,0), and $(\infty, 0)$] and four armchair CNTs [(4,4), (5,5), (8,8), and (∞,∞)]. The diameter for each CNT is marked for the corresponding curve, and $(\infty, 0)$ and (∞, ∞) correspond to a graphene sheet with the direction of tension parallel and normal to a carbon bond, respectively. The curves for armchair CNTs display little dependence on the CNT radius R. The dependence on R is somewhat stronger for zigzag CNTs, but the overall influence of CNT radius is much less than that of CNT orientation. It is observed that, for the same range of CNT diameters, all curves for armchair CNTs are much higher than their counterpart for zigzag CNTs such that armchair CNTs have larger resistance against

tension. Therefore, the effect of CNT radius is secondary as compared to CNT orientation.

5. A single wall carbon nanotube in pure torsion

Let κ denote the twist (angle of rotation per unit length) for a CNT in pure torsion, and R and r the CNT radius in the undeformed and deformed configurations, respectively. The cylindrical coordinates of a material point on the CNT are (R, Θ, Z) prior to deformation, and become (r, θ, z) under torsion, where $\theta = \Theta + \kappa Z$, $z = (1+\varepsilon)Z$, and ε is the axial strain due to the finite deformation.

The base vectors $\boldsymbol{e}_r$, $\boldsymbol{e}_\theta$, and $\boldsymbol{e}_z$ in the cylindrical coordinates for the deformed configuration are related to their counterparts $\boldsymbol{e}_R$, $\boldsymbol{e}_\Theta$, and $\boldsymbol{e}_Z$ in the undeformed configuration by $\boldsymbol{e}_r = \cos\kappa Z\boldsymbol{e}_R + \sin\kappa Z\boldsymbol{e}_\Theta$, $\boldsymbol{e}_\theta = -\sin\kappa Z\boldsymbol{e}_R + \cos\kappa Z\boldsymbol{e}_\Theta$, and $\boldsymbol{e}_z = \boldsymbol{e}_Z$. The deformation gradient for pure torsion (a material point moving from $R\boldsymbol{e}_R + Z\boldsymbol{e}_Z$ to $r\boldsymbol{e}_r + z\boldsymbol{e}_z$) is given by

$$\begin{aligned}\boldsymbol{F} &= \frac{r}{R}\boldsymbol{e}_\theta\boldsymbol{e}_\Theta + \kappa r\boldsymbol{e}_\theta\boldsymbol{e}_Z + (1+\varepsilon)\boldsymbol{e}_z\boldsymbol{e}_Z \\ &= \frac{r}{R}(-\sin\kappa Z\boldsymbol{e}_R + \cos\kappa Z\boldsymbol{e}_\Theta)\boldsymbol{e}_\Theta + \kappa r(-\sin\kappa Z\boldsymbol{e}_R \\ &\quad + \cos\kappa Z\boldsymbol{e}_\Theta)\boldsymbol{e}_Z + (1+\varepsilon)\boldsymbol{e}_Z\boldsymbol{e}_Z. \end{aligned} \tag{38}$$

The Lagrangian strain $\boldsymbol{E}$ is found from (19) as

$$\begin{aligned}\boldsymbol{E} &= \frac{1}{2}\left(\frac{r^2}{R^2} - 1\right)\boldsymbol{e}_\Theta\boldsymbol{e}_\Theta + \frac{\kappa}{2}\frac{r^2}{R}(\boldsymbol{e}_\Theta\boldsymbol{e}_Z + \boldsymbol{e}_Z\boldsymbol{e}_\Theta) \\ &\quad + \frac{1}{2}(\kappa^2 r^2 + 2\varepsilon + \varepsilon^2)\boldsymbol{e}_Z\boldsymbol{e}_Z. \end{aligned} \tag{39}$$

The non-vanishing components of the second Piola–Kirchhoff stress are $T_{\Theta\Theta}$, T_{ZZ}, and $T_{\Theta Z}$ $(= T_{Z\Theta})$, and they are independent of Θ for a CNT in pure torsion. The equilibrium equation (31) projected along $\boldsymbol{e}_r$, $\boldsymbol{e}_\theta$ and $\boldsymbol{e}_z$ directions becomes

$$F_{\theta\Theta}T_{\Theta\Theta} + F_{\theta Z}T_{\Theta Z} + \kappa R(F_{\theta\Theta}T_{\Theta Z} + F_{\theta Z}T_{ZZ}) = 0, \tag{40a}$$

$$\frac{\mathrm{d}}{\mathrm{d}Z}(F_{\theta\Theta}T_{\Theta Z} + F_{\theta Z}T_{ZZ}) = 0, \tag{40b}$$

$$\frac{\mathrm{d}}{\mathrm{d}Z}(F_{zZ}T_{ZZ}) = 0. \tag{40c}$$

The substitution of the deformation gradient in (38) into (40) yields

$$T_{ZZ} = \text{constant}, \quad T_{\Theta Z} = \text{constant}, \tag{41a}$$

$$T_{\Theta\Theta} = -2\kappa R T_{\Theta Z} - \kappa^2 R^2 T_{ZZ}. \tag{41b}$$

The boundary condition in pure torsion requires the normal stress traction to vanish at the two end sections of the CNT, $\boldsymbol{e}_z \cdot (\boldsymbol{F}\cdot\boldsymbol{T}\cdot\boldsymbol{e}_Z) = 0$, which gives $T_{ZZ} = 0$ at the two ends. Therefore, (41) becomes

$$T_{\Theta\Theta} = -2\kappa R T_{\Theta Z}, \quad T_{ZZ} = 0 \tag{42}$$

in the entire CNT. They are two implicit equations to determine the radius r and axial strain ε of the deformed CNT in terms of the twist κ.

The torque T on the CNT can be obtained by integrating the shear stress traction $\boldsymbol{e}_\theta \cdot (\boldsymbol{F}\cdot\boldsymbol{T}\cdot\boldsymbol{e}_Z)$ multiplied by the radius r of the deformed CNT, which gives

$$T = 2\pi r^2 T_{\Theta Z}, \tag{43}$$

where $T_{\Theta Z}$ is obtained from (27). Fig. 7 shows the torque T, normalized by the square of CNT radius

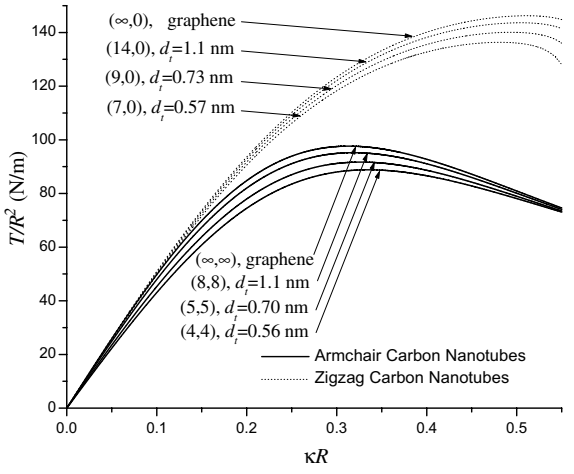

Fig. 7. The torque T, normalized the square of nanotube radius R^2 prior to deformation, versus the normalized twist κR for several zigzag and armchair carbon nanotubes in pure torsion. The diameter d_t of the carbon nanotube is given for each curve. The corresponding curves for graphene are also shown.

R^2, versus the normalized twist κR for the same four zigzag and four armchair CNTs as in Fig. 6. The curves for zigzag CNTs are relatively close, which suggest somewhat weak dependence on the CNT radius. The same conclusion also holds for armchair CNTs in Fig. 7. Similar to Fig. 6, the two sets of curves are far apart. This suggest once again that the effect of CNT orientation is significantly larger than that of CNT radius. It is also interesting to observe that, contrary to Fig. 6, the curves for zigzag CNTs are on top of those for armchair CNTs, indicating that zigzag CNTs have larger resistance against torsion.

6. Concluding remarks

We have examined the effect of nanotube radius on the constitutive model for carbon nanotubes (CNTs). Our analysis is based on the modified Cauchy–Born rule to incorporate the interatomic potential into a continuum analysis. The modification of the Cauchy–Born rule ensures the equilibrium of atoms. It is observed that, for CNTs in simple tension or in pure torsion, the influence of CNT orientation (e.g., zigzag versus armchair) is significant, but the CNT radius has little effect on the mechanical behavior of CNTs. Therefore, the simple constitutive model of [35,36], which neglects the effect of radius, can be used for CNTs. The proposed method has been applied to study the electrical property change of CNTs due to mechanical deformation [48], and the defect nucleation in CNTs in the form of Stones-Wales transformation [49].

Acknowledgements

Y.H. acknowledges the support from NSF (grants 00-99909 and 01-03257), Alexander von Humboldt Foundation, Center for Advanced Study at the University of Illinois, Urbana-Champaign, the NCSA/UIUC Faculty Fellow Program, and NSFC. H.G. acknowledges the support from NSF (grant 01-03257), NSFC and the Ministry of Education, China. K.C.H. acknowledges support from NSFC and the Ministry of Education, China.

Appendix A

We show that the sequence of deforming a carbon nanotube (CNT) and "unrolling" the deformed CNT to a plane can be exchanged, i.e., it is equivalent to first "unrolling" the undeformed CNT to a plane and then deforming the plane according to $E_{11} = E_{\Theta\Theta}$, $E_{22} = E_{ZZ}$, and $E_{12} = E_{21} = E_{\Theta Z} (= E_{Z\Theta})$. For simplicity, we show the above conclusion for simple tension, though it also holds for pure torsion.

Let d_t and L denote the diameter and length of a carbon CNT. For given components $E_{\Theta\Theta}$ and E_{ZZ} of the Lagrangian strain, the deformation gradient is $F_{\Theta\Theta} = \sqrt{1 + 2E_{\Theta\Theta}}$ and $F_{ZZ} = \sqrt{1 + 2E_{ZZ}}$. The diameter and length of the deformed CNT are $d_t F_{\Theta\Theta}$ and LF_{ZZ}, respectively. The "unrolling" of such a cylinder gives a rectangle whose length and height are $\pi d_t F_{\Theta\Theta}$ and LF_{ZZ}, respectively.

If we "unroll" the undeformed CNT first, the length and height of the resulting rectangle are πd_t and L, respectively. Once the in-plane Lagrangian strain components E_{11} and E_{22} are imposed, it is straightforward to show that $E_{11} = E_{\Theta\Theta}$ and $E_{22} = E_{ZZ}$ ensures the sequence of the above two operators can be exchanged.

References

[1] S. Iijima, Helical microtubules of graphite carbon, Nature 354 (1991) 56–58.
[2] M.M.J. Treacy, T.W. Ebbesen, J.M. Gibson, Exceptionally high Young's modulus observed for individual carbon nanotubes, Nature 381 (1996) 678–680.
[3] A. Krishnan, E. Dujardin, T.W. Ebbesen, P.N. Yianilos, M.M.J. Treacy, Young's modulus of single-walled nanotubes, Physical Review B 58 (1998) 14013–14019.
[4] E.W. Wong, P.E. Sheehan, C.M. Lieber, Nanobeam mechanics: Elasticity, strength, and toughness of nanorods and nanotubes, Science 277 (1997) 1971–1975.
[5] J.-P. Salvetat, G.A.D. Briggs, J.-M. Bonard, R.R. Bacsa, A.J. Kulik, Elastic and shear moduli of single-walled carbon nanotube ropes, Physical Review Letters 82 (1999) 944–947.
[6] T.W. Tombler, C. Zhou, L. Alexseyev, J. Kong, H. Dai, L. Liu, C.S. Jayanthi, M. Tang, S.-Y. Wu, Reversible electromechanical characteristics of carbon nanotubes under local-probe manipulation, Nature 405 (2000) 769–772.
[7] M.-F. Yu, B.S. Files, S. Arepalli, R.S. Ruoff, Tensile loading of ropes of single wall carbon nanotubes and their

mechanical properties, Physical Review Letters 84 (2000) 5552–5555.
[8] M.-F. Yu, M.J. Dyer, G.D. Skidmore, H.W. Rohrs, X. Lu, K.D. Ausman, J.R. von Ehr, R.S. Ruoff, Three-dimensional manipulation of carbon nanotubes under a scanning electron microscope, Nanotechnology 10 (1999) 244–252.
[9] J. Muster, M. Burghard, S. Roth, G.S. Duesberg, E. Hernández, A. Rubio, Scanning force microscopy characterization of individual carbon nanotubes on electrode arrays, Journal of Vacuum Science and Technology B 16 (1998) 2796–2801.
[10] O. Lourie, H.D. Wagner, Evaluation of young's modulus of carbon nanotubes by micro-raman spectroscopy, Journal of Materials Research 13 (1998) 2418–2422.
[11] Z.W. Pan, S.S. Xie, L. Lu, B.H. Chang, L.F. Sun, W.Y. Zhou, G. Wang, D.L. Zhang, Tensile tests of ropes of very long aligned multiwall carbon nanotubes, Applied Physics Letters 74 (1999) 3152–3154.
[12] D.H. Robertson, D.W. Brenner, J.W. Mintmire, Energetics of nanoscale graphitic tubules, Physical Review B 45 (1992) 12592–12595.
[13] G. Overney, W. Zhong, D. Tománek, Structural rigidity and low-frenquency vibrational modes of long carbon tubules, Zeitschrift für Physik D: Atoms, Molecules and Clusters 27 (1993) 93–96.
[14] J.M. Molina, S.S. Savinsky, N.V. Khokhriakov, A tight-binding model for calculations of structures and properties of graphitic nanotubes, Journal of Chemical Physics 104 (1996) 4652–4656.
[15] B.I. Yakobson, C.J. Brabec, J. Bernholc, Nanomechanics of carbon tubes: Instabilities beyond linear response, Physical Review Letters 76 (1996) 2511–2514.
[16] C.F. Cornwell, L.T. Wille, Elastic properties of single-walled carbon nanotubes in compression, Solid State Communications 101 (1997) 555–558.
[17] J.P. Lu, Elastic properties of carbon nanotubes and nanoropes, Physical Review Letters 79 (1997) 1297–1300.
[18] T. Halicioglu, Stress calculations for carbon nanotubes, Thin Solid Films 312 (1998) 11–14.
[19] E. Hernández, C. Goze, P. Bernier, A. Rubio, Elastic properties of C and $B_xC_yN_z$ composite nanotubes, Physical Review Letters 80 (1998) 4502–4505.
[20] E. Hernández, C. Goze, P. Bernier, A. Rubio, Elastic properties of single-wall nanotubes, Applied Physics A 68 (1999) 287–292.
[21] C. Goze, L. Vaccarini, L. Henrard, P. Bernier, E. Hernandez, A. Rubio, Elastic and mechanical properties of carbon nanotubes, Synthetic Metals 103 (1999) 2500–2501.
[22] D. Sánchez-Portal, E. Artacho, J.M. Soler, A. Rubio, P. Ordejón, Ab Initio structural, elastic, and vibrational properties of carbon nanotubes, Physical Review B 59 (1999) 12678–12688.
[23] G.V. Lier, C.V. Alsenoy, V.V. Doran, P. Geerlings, Ab initio study of the elastic properties of single-walled carbon nanotubes and graphene, Chemical Physics Letters 326 (2000) 181–185.
[24] V.N. Popov, V.E. van Doren, M. Balkanski, Elastic properties of single-walled carbon nanotubes, Physical Review B 61 (2000) 3078–3084.
[25] Y.I. Prylutskyy, S.S. Durov, O.V. Ogloblya, E.V. Buzaneva, P. Scharff, Molecular dynamics simulations of mechanical, vibrational and electronic properties of carbon nanotubes, Computational Materials Science 17 (2000) 352–355.
[26] L. Vaccarini, C. Goze, L. Henrard, E. Hernández, P. Bernier, A. Rubio, Mechanical and electronic properties of carbon and boron-nitride nanotubes, Carbon 38 (2000) 1681–1690.
[27] G. Zhou, W. Duan, B. Gu, First-principles study on morphology and mechanical properties of single-walled carbon nanotube, Chemical Physics Letters 333 (2001) 344–349.
[28] E.B. Tadmor, M. Ortiz, R. Philips, Quasicontinuum analysis of defects in solids, Philosophical Magazine A 73 (1996) 1529–1563.
[29] E.B. Tadmor, R. Philips, M. Ortiz, Mixed atomistic and continuum models of deformation in solids, Langmuir 12 (1996) 4529–4534.
[30] E.B. Tadmor, G.S. Smith, N. Bernstein, E. Kaxiras, Mixed finite element and atomistic formulation for complex crystals, Physical Review B 59 (1999) 235–245.
[31] H. Gao, P.A. Klein, Numerical simulation of crack growth in an isotropic solid with randomized internal cohesive bonds, Journal of the Mechanics and Physics of Solids 46 (1998) 187–218.
[32] P.A. Klein, H. Gao, Crack nucleation and growth as strain localization in a virtual-bond continuum, Engineering Fracture Mechanics 61 (1998) 21–48.
[33] G. Friesecke, R.D. James, A scheme for the passage from atomic to continuum theory for thin films, nanotubes and nanorods, Journal of the Mechanics and Physics of Solids 48 (2000) 1519–1540.
[34] M. Arroyo, T. Belytschko, An atomistic-based finite deformation membrane for single layer crystalline films, Journal of the Mechanics and Physics of Solids 50 (2002) 1941–1977.
[35] P. Zhang, Y. Huang, P.H. Geubelle, K.C. Hwang, On the continuum modeling of carbon nanotubes, Acta Mechanica Sinica 18 (2002) 528–536.
[36] P. Zhang, Y. Huang, P.H. Geubelle, P.A. Klein, K.C. Hwang, The elastic modulus of single-wall carbon nanotubes: A continuum analysis incorporating interatomic potentials, International Journal of Solids and Structures 39 (2002) 3893–3906.
[37] P. Zhang, H. Jiang, Y. Huang, P.H. Geubelle, K.C. Hwang, An atomistic-based continuum theory for carbon nanotubes: Analysis of fracture nucleation, Journal of the Mechanics and Physics of Solids (in press).
[38] Y. Huang, Z.L. Wang, Mechanics of carbon nanotubes, in: B. Karihaloo, R. Ritchie, I. Milne (Eds.), Comprehensive Structural Integrity Handbook, in: W. Gerberwich, W. Yang (Eds.), Interfacial and Nanoscale Fracture, vol. 8, Elsevier Science, 2003, pp. 551–579, Chapter 8.16.

[39] M. Born, K. Huang, Dynamical Theory of the Crystal Lattices, Oxford University Press, Oxford, 1954.
[40] F. Milstein, Review: theoretical elastic behaviour at large strains, Journal of Material Science 15 (1980) 1071–1084.
[41] J.H. Weiner, Statistical Mechanics of Elasticity, John Wiley & Sons, New York, 1983.
[42] D.W. Brenner, Empirical potential for hydrocarbons for use in simulating the chemical vapor deposition of diamond films, Physical Review B 42 (1990) 9458–9471.
[43] B.I. Yakobson, M.P. Campbell, C.J. Brabec, J. Bernholc, High strain rate fracture and C-chain unraveling in carbon nanotubes, Computational Materials Science 8 (1997) 341–348.
[44] P. Zhang, Y. Huang, H. Gao, K.C. Hwang, Fracture nucleation in single-wall carbon nanotubes under tension: a continuum analysis incorporating interatomic potentials, Journal of Applied Mechanics 69 (2002) 454–458.
[45] M.S. Dresselhaus, R.A. Jishi, G. Dresselhaus, D. Inomata, K. Nakao, R. Saito, Group theoretical concepts for carbon nanotubes, Molecular Materials 4 (1994) 27–40.
[46] D. Sánchez-Portal, E. Artacho, J.M. Soler, Ab initio structure, elastic, and vibrational properties of carbon nanotubes, Physical Review B 59 (1999) 12678–12688.
[47] B.I. Yakobson, P. Avouris, Mechanical properties of carbon nanotubes, in: M.S. Dresselhaus, G. Dresselhaus, P. Avouris (Eds.), Carbon Nanotubes, Vol. 80 of Topics in Applied Physics, 2001, pp. 287–329.
[48] B. Liu, H. Jiang, H.T. Johnson, Y. Huang, The influence of mechanical deformation on the electrical properties of single wall-carbon nanotubes, Journal of the Mechanics and Physics of Solids (in press).
[49] H. Jiang, X.Q. Feng, Y. Huang, K.C. Hwang, P.D. Wu, Defect nucleation in carbon nanotubes under tension and torsion: Stone-Wales transformation, Computer Methods in Applied Mechanics and Engineering (in press).